Contribution of Local and Remote Anthropogenic Aerosols to the 20th century Weakening of the South Asian Monsoon

Massimo A. Bollasina[1,2], Yi Ming[3], V. Ramaswamy[3], M. Daniel Schwarzkopf[3], and Vaishali Naik[4]

[1]Program in Atmospheric and Oceanic Sciences, Princeton University, Princeton

[2]School of GeoSciences, University of Edinburgh[3]Geophysical Fluid Dynamics Laboratory/NOAA, Princeton

[4]UCAR/NOAA Geophysical Fluid Dynamics Laboratory, Princeton

Submitted to *Geophysical Research Letters* on September 30, 2013, revised on December 24, 2013

Corresponding author:

Massimo A. Bollasina

School of GeoSciences, University of Edinburgh

Grant Institute, The King's Bulldings, West Mains Road, Edinburgh EH9 1TB, UK

E-mail: massimo.bollasina@ed.ac.uk

Abstract

The late 20th century response of the South Asian monsoon to changes in anthropogenic aerosols from local (i.e., South Asia) and remote (i.e., outside South Asia) sources was investigated using historical simulations with a state-of-the-art climate model. The observed summertime drying over India is replaced by widespread wettening once local aerosol emissions are kept at pre-industrial levels while all the other forcings evolve. Constant remote aerosol emissions partially suppress the precipitation decrease. While predominant precipitation changes over India are thus associated with local aerosols, remote aerosols contribute as well, especially in favoring an earlier monsoon onset in June and enhancing summertime rainfall over the northwestern regions. Conversely, temperature and near-surface circulation changes over South Asia are more effectively driven by remote aerosols. These changes are reflected into northward cross-equatorial anomalies in the atmospheric energy transport induced by both local and, to a greater extent, remote aerosols.

1. Introduction

In the past decades emissions of anthropogenic aerosols over South Asia have dramatically increased due to rapid urbanization and population growth [e.g., *Ramanathan et al.*, 2008]. Atmospheric aerosols influence climate by modulating radiation in the atmosphere through scattering and absorption (the direct effect), and by altering cloud microphysical processes (the indirect effects). Their potential impact on the South Asian monsoon is an issue of highest relevance as about 20% of the world population heavily relies on monsoon precipitation for their livelihood, health, and economy.

Growing evidence from observational and modeling studies suggests that increased anthropogenic aerosols may have had a strong impact on the South Asian monsoon [e.g., *Menon et al.*, 2002; *Ramanathan et al.*, 2005; *Lau et al.*, 2006; *Meehl et al.*, 2008; *Wang et al.*, 2009; *Bollasina et al.*, 2011; *Cowan and Cai* 2011; *Ganguly et al.*, 2012; *Bollasina et al.*, 2013]. Aerosols are likely responsible for the observed late 20th century summertime drying over South Asia [e.g., *Bollasina et al.*, 2011]. However, the details of the physical pathway underlying the aerosol-monsoon link are not entirely clear [e.g., *Ganguly et al.*, 2012].

An important and rather unexplored topic is the extent to which increased anthropogenic aerosols from either local or remote sources contribute to long-term monsoon changes. Given the spatial extent of the South Asian monsoon, the influence of aerosols from surrounding heavily polluted regions (e.g., East Asian megacities) is plausible. Using coupled model historical simulations, *Cowan and Cai* [2011] concluded that Asian aerosols only weakly suppressed monsoon precipitation over the 20th century, and showed that a far greater reduction was obtained only after including also non-Asian aerosols (though their impact was not separately addressed). On the contrary, using equilibrium simulations with an atmosphere-slab ocean model *Ganguly et al.* [2012] found a major contribution to regional precipitation reduction from Asian anthropogenic aerosols. It is worth noting that in both studies the area of imposed Asian aerosol emissions extends over the domains of both the South Asian and East Asian monsoons. This might in part preclude a proper attribution of the impact of regional aerosols as there are several fundamental differences between the two Asian monsoon subsystems.

The goal of this study is to shed further light on this highly complex issue and to advance the understanding of the underlying aerosol mechanisms by using a state-of-the-art climate model and an improved experimental setting for the simulations. We used the U.S. National Oceanic and Atmospheric Administration (NOAA) Geophysical Fluid Dynamics Laboratory (GFDL) CM3 coupled model, which has fully-interactive aerosols and chemistry, and a representation of both direct and indirect aerosol effects [*Donner et al.*, 2011]. Three targeted historical (1860-2005) experiments, each a three-member ensemble, were carried out to assess the contribution of anthropogenic aerosols emitted by either local or remote sources to the long-term variation of the South Asian monsoon. The reference experiment is an all-forcing simulation (ALLF) with time-evolving natural (solar variations and volcanic aerosols) and anthropogenic (well-mixed greenhouse gases, ozone, aerosols, and land use) forcing agents. The two other experiments are identical to ALLF except for having time-evolving anthropogenic (including biomass burning) emissions of sulfur dioxide (SO_2), black carbon (BC) and organic carbon (OC) only from either South Asian countries (i.e., emissions from non-South Asian countries kept at 1860 (pre-industrial) levels, see Fig. 1c; hereafter PI_RW) or the rest of the world (i.e., South Asian emissions kept at 1860 levels; PI_SA). Aerosol emissions are based on *Lamarque et al.* [2010]. We focus on the observed 1950-1999 drying of the South Asian monsoon, whose characteristics are skillfully simulated by the model [*Bollasina et al.*, 2011; *Bollasina et al.*, 2013]. These experiments allow us to interpret the aerosol-related changes in the context of an evolving climate (i.e., in presence of other simultaneous forcing agents) and to ascertain whether the monsoon weakening would have occurred with either local or remote aerosol emissions held constant. Trends were calculated using a linear least-squares fit, and their statistical significance assessed by a two-tail Student *t*-test accounting for temporal autocorrelation.

2. South Asian monsoon response to local and remote anthropogenic aerosols

Figure 1 represents the 1950-1999 annual mean trend of total aerosol optical depth (AOD) in the ALLF, PI_SA, and PI_RW experiments. This is indistinguishable from the anthropogenic-only AOD trend, as the variation of natural aerosols is negligible. In the ALLF experiment the largest changes in AOD are found over northern India, Eastern China, and Southeast Asia (Fig. 1a). Outside Asia, aerosol burden markedly increased over equatorial Africa and decreased over northern Europe. The aerosol hotspots well correspond to areas where large changes of anthropogenic aerosol emissions occurred (Fig. S1), although, once emitted, aerosols are also transported to nearby regions (e.g., over Central Asia by the midlatitude westerlies). The increase in SO_2 and BC emissions over northern India and eastern China is large, and is associated with the rapid rise in fossil fuel burning due to steady economic growth. Using *Lamarque et al.* [2010] inventories, SO_2 and BC emissions respectively increased about sixteen-fold and five-fold in East Asia, and about ten-fold and two-fold in South Asia during the period 1950-2000 (Fig. S1; *Ramanathan et al.*, 2008]. Note that the relative growth in emissions of the two species does not translate directly into their importance for radiative forcing due to surface and cloud reflective effects [e.g., *Haywood and Ramaswamy*, 1998]. The increase of OC over Southeast Asia and Africa is also substantial. Conversely, European and North American aerosol emissions peaked in the 1970s and started to decrease significantly since then [e.g., *Lamarque et al.*, 2010].

Emissions from outside South Asia also contribute to increasing regional AOD, especially due to the westward transport of Southeast Asian aerosols over the eastern Indian Ocean (Fig. 1b). In turn, aerosols resulting from South Asian sources tend to spread over the north-equatorial Indian Ocean and toward Southeast Asia (Fig. 1c). The changes in AOD are to a good approximation linearly additive between PI_SA and PI_RW to produce the ALLF pattern.

The ALLF summertime precipitation change over South Asia is shown in Figure 2a. The monsoon underwent a remarkable drying over central-northern India and Indochina [e.g., *Bollasina et al.*, 2011], which is reasonably well simulated by the model. The model also captures the wettening over northwestern India, Pakistan and the surrounding western north-equatorial Indian Ocean. Note that, for consistency among the experiments, three members are averaged in Fig. 2a and not five as in Fig. 2 of *Bollasina et al.* [2011], which explains some minor differences between the two plots. Figures 2b-c display the precipitation trends in PI_SA and PI_RW, respectively. Preventing South Asian aerosols to increase leads to wetter conditions over India, offsetting the dry anomaly to the northeast (Fig. 2b). With remote aerosols at pre-industrial levels precipitation slightly decreases over northern and central India, and the wettening over the northwestern regions almost disappears (Fig. 2c). The 50-year changes averaged over central-northern India (the orange box in Fig. 2, as used in *Bollasina et al.* [2011]) are -0.81, +0.24, and -0.41 mm day^{-1} for ALLF, PI_SA, and PI_RW, respectively. If for a moment we neglect non-linearities among the various forcings [e.g., *Ming and Ramaswamy*, 2009] and subtract each aerosol experiment from ALLF, these findings suggest that both local and remote aerosols are effective in reducing precipitation over India, with the former exerting the predominant impact (-1.05 and -0.40 mm day^{-1} for the difference ALLF-PI_SA and ALLF-PI_RW, respectively). An opposite picture appears over the eastern Bay of Bengal and Southeast Asia, where the precipitation decline is unaltered in PI_SA but is largely reduced in PI_RW. Noteworthy are also the opposite changes along the equatorial Indian Ocean between PI_SA and PI_RW, suggesting the existence of a consistent large-scale pattern linking continental and oceanic anomalies.

Noticeable changes occurred also in the monsoon seasonality over India, specifically a shift toward an earlier onset [*Bollasina et al.* 2013]. In the ALLF experiment the anticipated onset manifests as an area of slight precipitation increase over northeastern India during May, which gradually expands and moves westward in June while being replaced by precipitation decline to the northeast (Fig. 2d). Keeping local aerosols at pre-industrial levels mainly affects June precipitation over the northeast, where the ALLF reduction is offset by a large precipitation increase (Fig. 2e). Conversely, constant remote aerosols almost entirely abate the June precipitation increase over central and northwestern India (Fig. 2f). This suggests aerosols outside South Asia to be the primary driver of the onset shift, supporting the findings of *Bollasina et al.* [2013] on the importance of spring aerosol forcing over the eastern equatorial Indian Ocean for the earlier monsoon development.

Changes in precipitation are associated with variations in other near-surface variables, as displayed in Figure 3. The ALLF widespread cooling over South Asia (Fig. 3a) indicates the predominance of aerosol dimming over greenhouse gas warming. The warming prevails over the Middle East and the western equatorial Indian Ocean. In fact, areas of larger temperature decrease tend to be collocated with areas of higher AOD (Fig. 1), although the cooling is not necessarily restricted to the aerosol source regions due to feedbacks with circulation changes [e.g., *Ming and Ramaswamy*, 2012]. The associated anomalous southwest-northeast sea level pressure gradient toward the Indian subcontinent hinders the climatological monsoon southwesterlies. Simultaneously, the flow is deflected toward northwestern India and Pakistan, where it leads to precipitation increase.

The PI_SA ensemble features a large cyclonic circulation over northeastern Europe extending over the Middle East and central Asia (Fig. 3b). These changes are associated with declining aerosols over Europe and the emergence of greenhouse gas warming over the low-AOD areas in the Middle East and central Asia. Interestingly, this pattern is weaker in ALLF despite unaltered regional AOD, likely in response to changes in the monsoon remote forcing (see also Fig. S2b). Topographical effects by the Zagros Mountains might further accentuate the meandering of the flow over Iran (Fig. 3b). As a result, reinforced humid southwesterlies blow across the Arabian Sea leading to the continental precipitation increase (Fig. 2b). It is worth noting the similarity of the changes over Southeast Asia between PI_SA and ALLF.

Keeping non-South Asian aerosols constant leads to widespread warming over the whole domain, larger over Eurasia, but, interestingly, also over India despite the increase of regional aerosols (Fig. 3c). The northward temperature gradient induces a southward sea level pressure increase, with a large anticyclone stretching from the Middle East to the western Pacific. This causes an easterlies to blow across the Indian Ocean, confining the monsoon front at the equator. A weaker westerly moisture transport over Burma compared to the climatology leads to a slight precipitation decrease.

The analysis of the trends in the upper tropospheric divergent circulation provides a link between surface and three-dimensional atmospheric circulation changes (Fig. 4). Comparison with Fig. 2 shows an excellent qualitative agreement between areas of upper tropospheric divergence (negative velocity potential) and precipitation increase. The ALLF pattern (Fig. 4a) is essentially composed of two zonal cells along the equator and at about 30°N, as well as of a transverse circulation from the western Indian Ocean to Indochina. The PI_SA outflow over India is predominantly heading westward, while the transverse circulation is largely suppressed (Fig. 4b). Conversely, the equatorial outflow in PI_RW reinforces the eastward and northward cells across the Indian subcontinent, with no appreciable westward flow (Fig. 4c). The impact of local and remote aerosols on the divergent circulation thus extends beyond their source regions with changes prevalently in opposite directions.

Figure 4d shows the trends in the meridional atmospheric energy transport. Previous work indicated that aerosols, mainly concentrated in the northern hemisphere, induced an anomalous cross-equatorial northward transport in order to compensate for the interhemispheric top-of-the-atmosphere energy imbalance [*Bollasina et al.*, 2011]. Changes are discernible in both PI_SA and PI_RW experiments. In PI_SA, the northward cross-equatorial energy export increases and extends to about 30°N compared to ALLF, as the energy deficit at low latitudes is smaller with pre-industrial South Asian aerosols. In PI_RW, the transport is reversed due to the increasingly larger warming from the southern tropics to the northern midlatitudes (Fig. 3c), and results in enhanced energy transport toward the southern hemisphere subtropics. This pattern bears substantial resemblance with the one induced by increased greenhouse gases alone (WMGG), although, very importantly, this has an even larger cross-equatorial southward flow. As a first order approximation (i.e., considering only the two strongest and long-term forcings on climate, greenhouse gases and aerosols, and assuming additivity), the difference between PI_SA (or PI_RW) and WMGG shows that, after accounting for the effect of global warming, both local and, to a greater extent, remote aerosols induce an anomalous northward cross-equatorial energy transport converging in the northern tropics.

3. Concluding remarks

Using a set of all-forcing historical experiments with a climate model in which either South Asian or non-South Asian anthropogenic aerosol emissions are kept at 1860s levels while other anthropogenic and natural forcings evolve, we found that both local and remote aerosols are important for explaining the late 20th century drying of the South Asian monsoon. Keeping non-South Asian aerosols constant result in a slight precipitation reduction across South Asia, indicating that part of the drying is attributable to remote aerosols. Conversely, Indian precipitation increases when South Asian aerosol sources are fixed, suggesting a predominant effect of local aerosols. Remote aerosols play an important role for precipitation enhancement over northwestern South Asia and, to a greater extent, the decline over Southeast Asia. Interestingly, temperature and lower-tropospheric wind over South Asia are more strongly affected by constant remote aerosols. These results highlight the complex interplay between aerosols from the two source regions through coupled feedbacks with circulation changes.

We acknowledge that there are uncertainties in aerosol emissions data, as well as in the model representation of aerosol effects, especially the indirect ones; both these aspects are relevant and need further improvement. We also note that in this model changes in dust emission occur only in response to variations in surface wind; in all three experiments, despite some differences due to a different near-surface circulation, dust AOD trends are negligible (less than ±0.004 over 50 years). A caveat of the present experimental setting, in which aerosol emissions vary on top of other evolving forcings, is that it does not allow a rigorous isolation of the individual contribution of local and remote aerosol sources (as in aerosol-only experiments) since non-linear feedbacks between aerosols and other forcing agents may feature prominently in the overall response [e.g., *Ming and Ramaswamy*, 2009]. Finally, given the large diabatic heating associated with the South Asian monsoon, South Asian anthropogenic aerosols might have also had a westward remote impact [e.g., *Kim et al.*, 2006; see also Fig. 3]. This important issue is currently largely unexplored.

Acknowledgements

The authors would like to thank Larry Horowitz, and David Paynter and Yuxing Yun for reviewing an earlier version of the manuscript, and an anonymous reviewer. M.A.B. was supported by the Princeton Environmental Institute with support from BP.

References

Bollasina, M., Y. Ming, and V. Ramaswamy (2011), Anthropogenic aerosols and the weakening of the South Asian summer monsoon, *Science*, *28*, 502-505, doi:10.1126/science.1204994.

Bollasina, M., Y. Ming, and V. Ramaswamy (2013), Earlier onset of the Indian monsoon in the late 20th century: the role of anthropogenic aerosols, *Geophys. Res. Lett., 40,* 3715-3720, doi: 10.1002/grl.50719.

Cowan, T., and W. Cai (2011), The impact of Asian and non-Asian anthropogenic aerosols on 20th century Asian summer monsoon, *Geophys. Res. Lett.*, *38*, L11703, doi:10.1029/2011GL047268.

Donner, L. J., et al. (2011), The dynamical core, physical parameterizations, and basic simulation characteristics of the atmospheric component AM3 of the GFDL global coupled model CM3. *J. Clim.*, *24*, 3484–3519. doi:http://dx.doi.org/10.1175/2011JCLI3955.1.

Ganguly, D., P. J. Rasch, H. Wang, and J.-H. Yoon (2012), Climate response of the South Asian monsoon system to anthropogenic aerosols, *J. Geophys. Res.*, *117*, D13209, doi:10.1029/2012JD017508.

Haywood, J. M. and V. Ramaswamy (1998), Global sensitivity studies of the direct radiative forcing due to anthropogenic sulfate and black carbon aerosols, *J. Geophys. Res.*, *103*, 6043-6058, doi: 10.1029/97JD03426.

Kim, M.-K., W. K. M. Lau, M. Chin, K.-M. Kim, Y. C. Sud, G. K. Walker (2006), Atmospheric teleconnection over Eurasia induced by aerosol radiative forcing during boreal spring, *J. Climate*, *19*, 4700–4718, doi: http://dx.doi.org/10.1175/JCLI3871.1.

Lamarque, J.-F., et al. (2010), Historical (1850-2000) gridded anthropogenic and biomass burning emissions of reactive gases and aerosols: Methodology and application, *Atmos. Chem. Phys.*, *10*, 7017-7039, doi:10.5194/acp-10-7017-2010.

Lau, W. K. M., and K.-M. Kim (2010), Fingerprinting the impacts of aerosols on long-term trends of the Indian summer monsoon regional rainfall, *Geophys. Res. Lett.*, *37*, L16705, doi:10.1029/2010GL043255.

Meehl, G. A., J. M. Arblaster, and W. D. Collins (2008), Effects of black carbon aerosols on the Indian monsoon, *J. Clim.*, *21*, 2869–2882, doi: http://dx.doi.org/10.1175/2007JCLI1777.1.

Menon, S., J. Hansen, L. Nazarenko, and Y. Luo (2002), Climate effects of black carbon aerosols in China and India, *Science*, *297*, 2250–2253.

Ming, Y., and V. Ramaswamy (2009), Nonlinear climate and hydrological responses to aerosol effects, *J. Climate*, *22*, 1329–1339, doi: http://dx.doi.org/10.1175/2008JCLI2362.1.

Ming, Y., and V. Ramaswamy (2012), Nonlocal component of radiative flux perturbation, *Geophys. Res. Lett.*, *39*, L22706, doi:10.1029/2012GL054050.

Ramanathan, V. et al. (2005), Atmospheric brown clouds: impacts on South Asian climate and hydrological cycle, *PNAS, 102*, 5326-5333.

Ramanathan, V. et al. (2008), Atmospheric Brown Clouds: Regional Assessment Report with Focus on Asia, published by the United Nations Environment Program, Nairobi, Kenya, pp. 1-360.

Wang, C., D. Kim, A. M. L. Ekman, M. C. Barth, and P. J. Rasch (2009), Impact of anthropogenic aerosols on Indian summer monsoon, *Geophys. Res. Lett.*, *36*, L21704, doi:10.1029/2009GL040114.

Figures

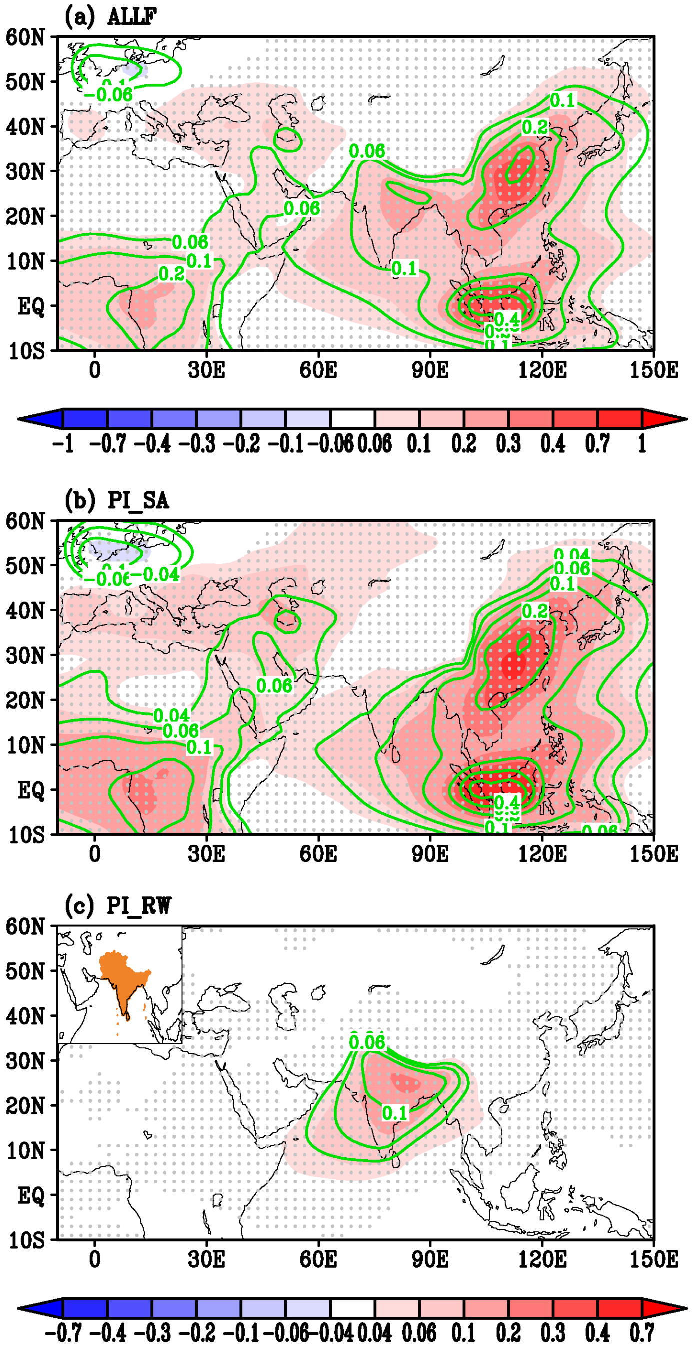

Figure 1: Spatial pattern of the 1950-1999 trends in annual mean AOD at 550 nm (changes over 50 years) for total aerosols (shaded) and absorbing aerosols only (x10, green contours) for (a) the all-forcing ensemble (ALLF), (b) the all-forcing experiment with fixed pre-industrial anthropogenic aerosol emissions over South Asia (PI_SA, which comprises Afghanistan, Bangladesh, Bhutan, India, Maldives, Nepal, Pakistan, and Sri Lanka; see the orange area in the inset of Fig. 1c), (c) the all-forcing experiment with fixed pre-industrial anthropogenic aerosol emissions over the rest of the world (PI_RW). The grey dots mark the grid points for which the

trend exceeds the 95% confidence level according to the two-tailed Student's *t*-test. Note the different color scale between Fig. 1a and Figs. 1b-c to account for slightly lower AOD values in PI_SA and PI_RW compared to ALLF.

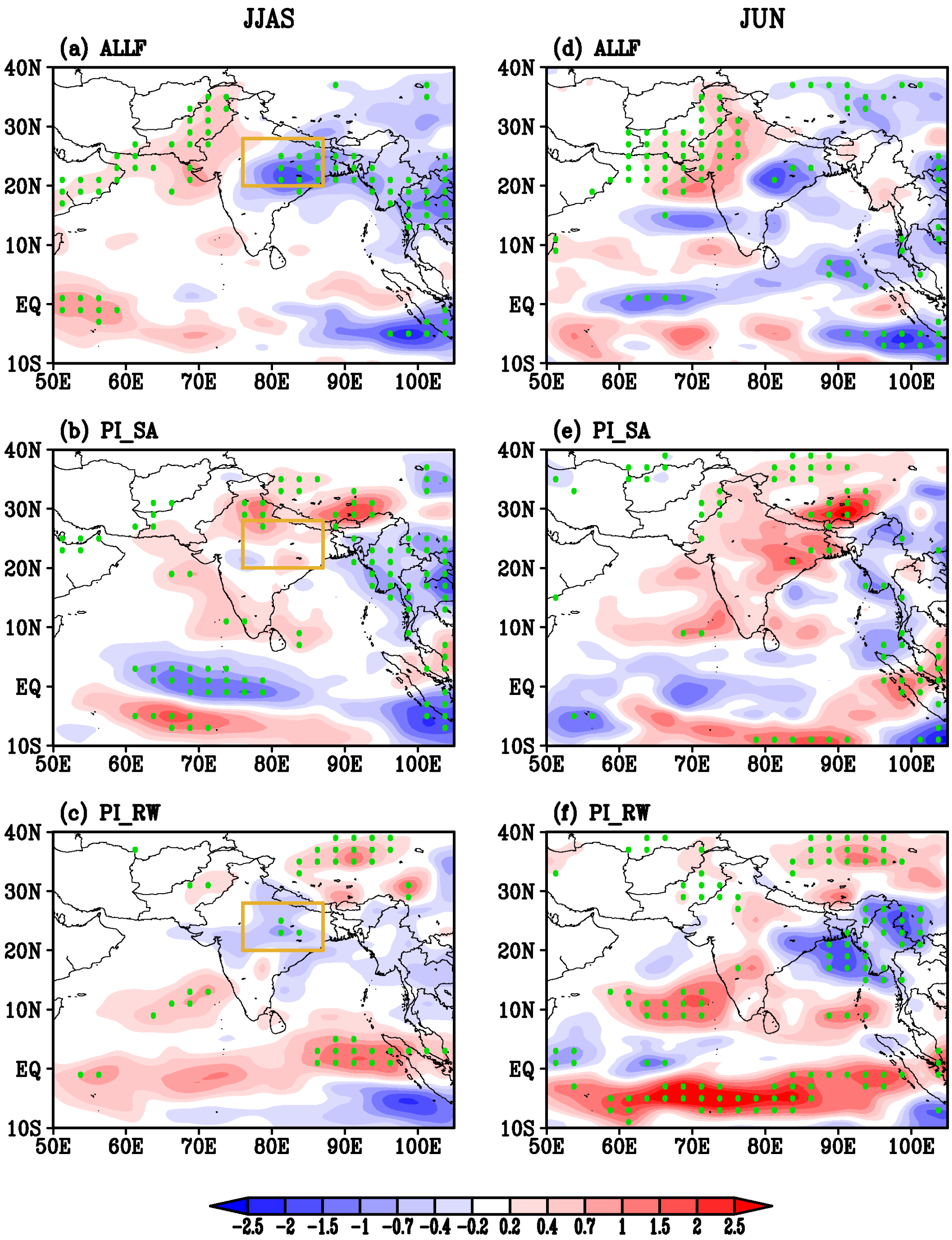

Figure 2: (a)-(c): As Figure 1, but for the trends in JJAS precipitation (mm day^{-1} (50 years)$^{-1}$). (d)-(f): As Figure 1, but for the trends in June precipitation (mm day^{-1} (50 years)$^{-1}$). The green dots mark the grid points for which the trend exceeds the 95% confidence level according to the two-tailed Student's *t*-test. The orange boxes in (a)-(c) denote the area of averaging for central-northern India (76°-87°E, 20°-28°N).

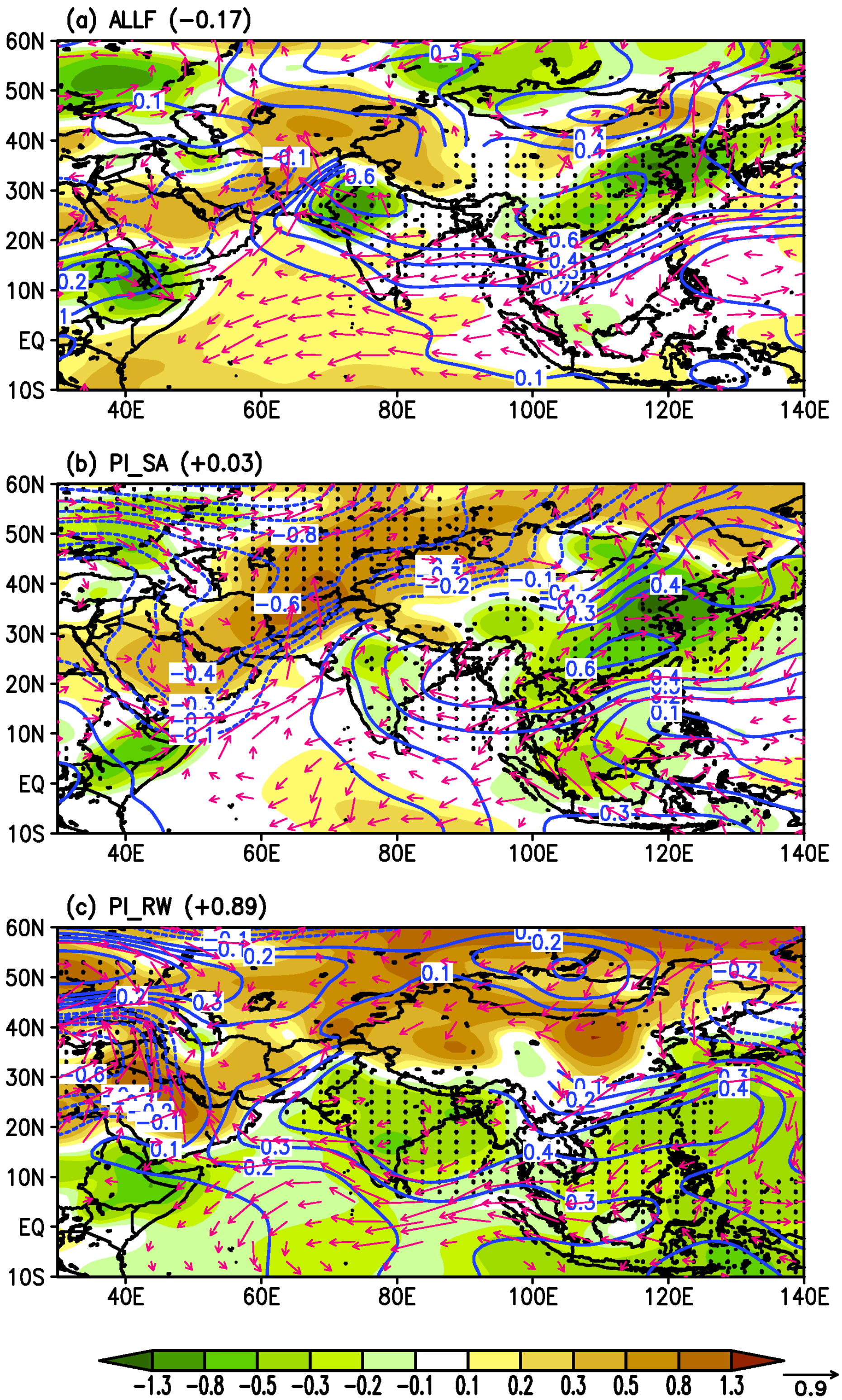

Figure 3: As Figure 1, but for the trends in JJAS surface temperature (K (50 years)$^{-1}$, shaded), sea level pressure (hPa (50 years)$^{-1}$, blue contours), and 850-hPa winds (m s^{-1} (50 years)$^{-1}$; vectors plotted when the magnitude of the change exceeds 0.2 m s^{-1}). Surface temperature

changes are plotted as residual after subtracting the domain-average change in each experiment, given in parenthesis at the top of each panel. The black dots mark the grid points for which the sea level pressure trend exceeds the 95% confidence level according to the two-tailed Student's *t*-test.

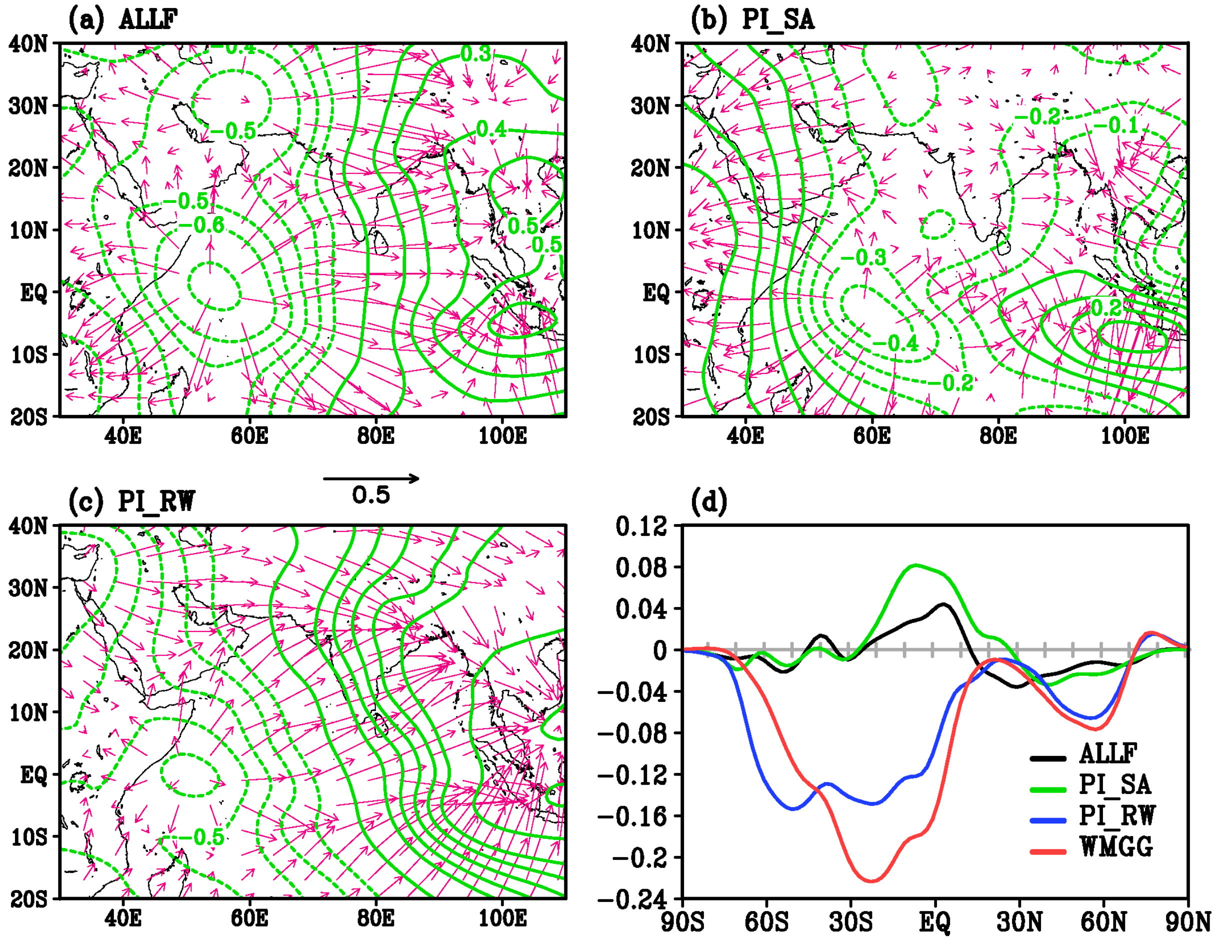

Figure 4: (a)-(c): As Figure 1, but for the trends in JJAS 200-hPa velocity potential (contours, x 106 m^2 s^{-1} (50 years)$^{-1}$) and divergent circulation (arrows, m s^{-1} (50 years)$^{-1}$). The divergent component of the circulation is computed by decomposing the horizontal wind into its divergent and rotational parts. (d): Change in the JJAS zonal mean vertically-integrated atmospheric energy transport (PW, northward transport is positive, 1 PW = 10^{15} W) over the period 1950-1999, computed as difference between decadal means at the beginning and end of the period (i.e., (1990-1999) minus (1945-1954), respectively). In addition to the experiments discussed above (ALLF, PI_SA, and PI_RW), a three-member ensemble historical experiment with greenhouse gases only forcing (WMGG; all other natural and anthropogenic forcing agents kept at pre-industrial levels) is also plotted for comparison.